Lin et al. *Zool. Res.* 2026, 47(1): 263−278
https://doi.org/10.24272/j.issn.2095-8137.2025.089
https://cstr.cn/32248.14.zr.2025.089

ZR | Zoological Research

Article Open Access

Epigenetic editing of marine medaka (*Oryzias melastigma*) *fgf2* using CRISPR/dCas9-Tet1CD

Lei Lin[1,2], Jing-Jing Zhang[1], Bing-Hua Liu[1], Sheng Du[1], Yang-Qing Zhang[1], Yu Yang[1], Chen Li[1], Cai-Chao Dong[1], Yang-Bin He[1], Qian Wang[1,3,4], Hong-Yan Wang[1,3,4,*], Chang-Wei Shao[1,3,4,*]

[1] *State Key Laboratory of Mariculture Biobreeding and Sustainable Goods*, *Yellow Sea Fisheries Research Institute*, *Chinese Academy of Fishery Sciences*, *Qingdao*, *Shandong* 266071, *China*

[2] *School of Graduate*, *Chinese Academy of Agricultural Sciences*, *Beijing* 100081, *China*

[3] *Laboratory for Marine Fisheries Science and Food Production Processes*, *Qingdao Marine Science and Technology Center*, *Qingdao*, *Shandong* 266237, *China*

[4] *Hebei Key Laboratory of the Bohai Sea Fish Germplasm Resources Conservation and Utilization*, *Beidaihe Central Experiment Station*, *Chinese Academy of Fishery Sciences*, *Qinhuangdao*, *Hebei* 066100, *China*

ABSTRACT

CRISPR/dCas9-mediated epigenetic editing offers a versatile approach for transcriptional regulation without introducing DNA strand breaks. Although this strategy has been explored in a limited number of species, its application in aquatic vertebrates remains largely uncharacterized. In this study, ten-eleven translocation methylcytosine dioxygenase 1 (*tet1*) was cloned and molecularly characterized in marine medaka (*Oryzias melastigma*). Decitabine treatment identified fibroblast growth factor 2 (*fgf2*) as a methylation-sensitive gene, with a regulatory CpG island located within its promoter region. Subsequently, a CRISPR/dCas9-Tet1CD activation system was constructed by fusing the catalytic domain of Tet1 (Tet1CD, Ala1352–Thr2034) to dCas9, enabling locus-specific DNA demethylation. Targeting *fgf2*, this CRISPR/dCas9-Tet1CD system induced efficient and selective demethylation of the CpG island, resulting in a maximal 2.41-fold increase in *fgf2* transcript levels. Whole-genome bisulfite sequencing and transcriptomic analysis confirmed high on-target precision with minimal off-target effects. Epigenetic activation of *fgf2* further modulated downstream gene networks associated with growth, promoting durable transcriptional enhancement and increased cellular proliferation. Collectively, these results establish a robust and highly specific epigenetic editing platform in marine medaka, providing a powerful tool for functional genomics studies and regulatory element analysis in aquatic models.

Keywords: Epigenetic editing; CRISPR/dCas9; Tet1; DNA demethylation; *fgf2*; *Oryzias melastigma*

INTRODUCTION

With rapid advancements in gene-editing technologies, clustered regularly interspaced short palindromic repeats (CRISPR)-based platforms have transformed genome engineering, progressively replacing earlier systems such as transcription activator-like effector nucleases and zinc finger nucleases (Gupta et al., 2019). By enabling efficient and precise gene modifications, CRISPR technologies have led to significant breakthroughs across biomedical research, therapeutic development, and agricultural innovation (Ahmad, 2023; Mani, 2021; Wang et al., 2022b; Zheng et al., 2024). In canonical applications, Cas9 endonuclease is directed by a guide RNA (gRNA) to a specific genomic locus, where it induces a double-strand DNA break, which is subsequently repaired via non-homologous end joining or homology-directed repair (Chae et al., 2023; Gupta et al., 2019; Liao et al., 2024). However, although widely adopted, this mechanism disrupts genome integrity and architecture, potentially undermining the precision of functional outcomes. Notably, emerging evidence indicates that CRISPR-induced genomic stress may confer a selective growth advantage to cells carrying specific mutations in DNA damage response pathways related genes, such as *TP53*, thereby enriching

Received: 13 June 2025; Accepted: 10 September 2025; Online: 11 September 2025

Foundation items: This work was supported by the National Key R&D Program of China (2022YFD2401500, 2022YFD2400100), Key Research and Development Project of Shandong Province (2024LZGC005), Taishan Scholars Program (tstp20221149), AoShan Talents Cultivation Program Supported by Qingdao National Laboratory for Marine Science and Technology (2017ASTCP-ES06), National Ten-Thousands Talents Special Support Program to C.W.S., Central Public-interest Scientific Institution Basal Research Fund, CAFS (2024XT0103, 2023TD19), and Key R&D Program of Hebei Province, China (21326307D)

*Corresponding authors, E-mail: wanghongyan@ysfri.ac.cn; shaocw@ysfri.ac.cn

potentially oncogenic subpopulations through impaired apoptotic clearance. This unexpected selective bias may increase the complexity of genome-editing applications, potentially favoring mutant clones during post-editing selection (Haapaniemi et al., 2018; Sinha et al., 2021).

Epigenetic modifications, particularly DNA methylation, constitute an essential layer of transcriptional regulation (Li et al., 2024b; Liu et al., 2025). Methylation of CpG islands within promoter regions is closely linked to gene silencing (de Mendoza et al., 2022). Notably, the ten-eleven translocation methylcytosine dioxygenase (TET) family plays a pivotal role in active DNA demethylation by catalyzing the oxidation of 5-methylcytosine (5mC) (Kohli et al., 2013). Among these, the demethylase TET1 has been extensively studied in mammalian systems for its roles in embryonic development, maintenance of stem cell pluripotency, and somatic cell reprogramming (Ito et al., 2010; Koh et al., 2011). Furthermore, TET1 mutations has emerged as a potential marker for tumor immune checkpoint inhibitor therapy (Wu et al., 2019).

Recently developed gene-editing platforms have enabled the reengineering of Cas9 into a catalytically inactive form, termed dead Cas9 (dCas9), which retains DNA-binding capability while lacking endonuclease activity (Qi et al., 2013). The specific targeting function is retained with the help of gRNA. For instance, dCas9 can be fused with epigenetic modification enzymes to modulate chromatin structure and regulate gene expression (Cappelluti et al., 2024). Epigenetic editing tools based on this approach have been applied in various disease models such as Alzheimer's disease and renal fibrosis (Park et al., 2022; Xu et al., 2018). In one study, CRISPR/dCas9-DNMT3a-mediated promoter methylation of the *app* gene effectively reduced amyloid-β production and alleviated memory impairment in an Alzheimer's model (Park et al., 2022). In mice, lentiviral delivery of dCas9-TET3CD reactivated two antifibrotic genes via targeted promoter demethylation, leading to attenuation of renal fibrosis and restoration of renal function (Xu et al., 2018). In fish, CRISPR/dCas9 epigenetic editing remains in the early stages of development. A limited number of studies have used dCas9 fused to methyltransferases (e.g., Dnmt7, Ezh2) or demethylases (e.g., Tet2) to modulate DNA methylation and histone modifications (Fukushima et al., 2019; Liang et al., 2023). Recently, we developed a CRISPR/dCas9-*dnmt3a* system in Chinese tongue sole (*Cynoglossus semilaevis*) and successfully increased DNA methylation in the *emx2* promoter region, leading to down-regulation of gene expression (Sun et al., 2024). These findings highlight the high specificity, durable effect, and low off-target risk of dCas9-based epigenetic tools (Nuñez et al., 2021), underscoring their broad potential in genetic research and therapeutic development. Nevertheless, validation and implementation of activation-based CRISPR/dCas9 epigenetic systems remain confined to a narrow range of taxa.

Marine medaka (*Oryzias melastigma*) has emerged as a tractable marine model due to its short generation time, transparent embryos and larvae, high genetic manipulation efficiency, and fully annotated genome (Kim et al., 2016). In the present study, a CRISPR/dCas9-based activation system was engineered by fusing the catalytic domain of Tet1 (Tet1CD) from *O. melastigma* to dCas9. Treatment with decitabine identified a CpG island within the fibroblast growth factor 2 (*fgf2*) promoter as a regulatory target. By targeting *fgf2*, the system exhibited high efficiency, specificity, and sustained activity. These findings establish a precise and effective CRISPR/dCas9 activation platform for targeted demethylation in marine medaka, providing a robust foundation for epigenetic studies and expanding its potential applications in marine teleost models.

MATERIALS AND METHODS

Collection and preparation of experimental fish, testis tissue, and primary testis cells

All *O. melastigma* individuals used in this study were laboratory-bred. Male fish were anesthetized with tricaine methanesulfonate (MS222, Merck, E10521, Germany) following protocols approved by the Institutional Animal Care and Use Committee (IACUC) to minimize procedural stress. Testis dissection and primary cell isolation were adapted from established protocols (Song & Gutzeit, 2003; Sun et al., 2024; Zhang et al., 2024a). Fish were dissected under sterile conditions using heat-sterilized instruments, and excised testicular tissues were cut into small pieces. A portion of the tissue was snap-frozen in liquid nitrogen and stored at –80°C for subsequent analyses. The remaining tissue was washed three times in serum-free medium under aseptic conditions to remove contaminants, then enzymatically digested with 0.25% trypsin-EDTA (Gibco, 25200072, USA) for 0.5 h. Digestion was monitored microscopically and terminated by adding complete medium. Cells were inoculated into culture flasks and maintained at 28°C in a cell culture incubator for one week. The culture medium was replaced every 3 days. Upon reaching confluence at approximately 10 days, cells were passaged using 1 mL of EDTA and 9 mL of culture medium to terminate digestion. The resulting suspension was divided equally into two culture flasks. Following a 3 days reattachment period, the culture was expanded. Primary testis cells were maintained for up to 10 passages.

Comparative and structural analysis of *tet1*

Amino acid sequences of TET1 orthologs from 25 species closely related to *O. melastigma*, along with representative model species, were retrieved from the NCBI database. Multiple sequence alignments were conducted using MEGA11 (Hall, 2013; Mello, 2018), and alignment visualizations were generated using ESPript v.3.0 (ibcp.fr) (Minh et al., 2020). A phylogenetic tree was constructed in MEGA11 using the neighbor-joining (NJ) method. Domain architectures of each protein were annotated using the NCBI Batch CD-Search tool (Lu et al., 2020; Wang et al., 2023) and visualized using the Conserved Domains Plot web interface. Conserved domain predictions of the TET1 protein across all 26 species were further confirmed using the NCBI Conserved Domain Search tool (nih.gov) (Wang et al., 2023). Protein motif analysis was conducted with the MEME Suite (https://meme-suite.org) (Bailey et al., 2015). Three-dimensional (3D) structure prediction for *O. melastigma* Tet1 was performed using the SWISS-MODEL server (https://swissmodel.expasy.org) (Waterhouse et al., 2018). The predicted structure was compared to the mouse TET1 reference model (AF-Q3URK3-F1-v4) from the AlphaFold Protein Structure Database using PyMOL v.2.5 (Delano, 2002).

Molecular cloning of *tet1* and construction of CRISPR/dCas9-Tet1CD expression plasmids

Amino and nucleic acid sequences of *O. melastigma* Tet1

were aligned using DNAMAN v.9.0, with conserved domain regions annotated. Primer pairs were designed using Primer v.5 software (Supplementary Table S1). Total RNA was extracted from *O. melastigma* testes using TRIzol reagent (Invitrogen, 15596026CN, USA), and cDNA was synthesized using a HiScript® III 1st Strand cDNA Synthesis Kit (+gDNA wiper) (Vazyme, R312-01, China). Polymerase chain reaction (PCR) amplification was performed using high-fidelity PrimeSTAR®Max DNA Polymerase (TAKARA, R045Q, Japan) in a 50 μL reaction containing 25 μL of PrimeSTAR Max Premix (2×), 2 μL of cDNA, 1.5 μL of forward and reverse primers, and 20 μL of DEPC-treated water. Cycling conditions were: pre-denaturation at 95°C for 5 min, followed by 35 cycles at 95°C for 15 s, 60°C for 1 min, and 72°C for 15 s. PCR products were separated by 1% agarose gel electrophoresis, and a ~1 000 bp band was excised, purified, ligated to the pEAZY-T1 vector (TransGen Biotech, CT101, China), and subjected to Sanger sequencing. The fuw-dCas9 plasmid (Addgene #84476, USA) (Liu et al., 2016) was linearized by digestion with BamH Ⅰ (NEB, R3136, USA) and EcoR Ⅰ (NEB, R0101, USA) at 37°C for 2 h. The digested plasmid and PCR-amplified *tet1* product were subsequently subjected to homologous recombination using ligase (Vazyme, C116-02, China) to generate a circular fuw-dCas9-Tet1 plasmid. The plasmid was extracted using an endotoxin-free TIANGEN Plasmid Extraction Kit (TIANGEN, DP118, China), and stored at –20°C.

Construction of single guide RNA (sgRNA) vectors

CpG islands within the *fgf2* promoter region were predicted using MethPrimer (urogene.org) (Li & Dahiya, 2002). Candidate sgRNA sites targeting CG-rich regions were designed using CRISPOR (ucsc.edu) (Concordet & Haeussler, 2018) and CCTop (Stemmer et al., 2015), with potential off-targets evaluated *in silico* (Supplementary Table S2). Selected forward and reverse primers were cloned into the pGL3-U6-sgRNA-PGK plasmid (Addgene #51133, USA) (Shen et al., 2014) using inverse PCR. Each 25 μL PCR reaction contained 12.5 μL of KOD (2× Master Mix, TOYOBO, KMM-101, Japan), 1 μL of sgRNA plasmid, 0.7 μL of forward and reverse primers, and 10.1 μL of DEPC-treated water. The thermocycling protocol included: 30 cycles at 98°C for 10 s, 50°C for 10 s, and 68°C for 10 s. Template DNA was removed by digestion with DpnI (NEB, R0176, USA) at 37°C for 30 min. Recombinant sgRNA plasmids were purified using the endotoxin-free TIANGEN Plasmid Extraction Kit and stored at –20°C.

Cell culture and transfection

Primary testis cells were seeded in 6-well plates and cultured in complete medium until reaching 70%–80% confluence (24 h). For transfection, Opti-MEM™ I Reduced Serum Medium (Thermo Fisher, 31985070, USA) was used in place of complete medium. To evaluate potential off-target effects of sgRNA-guided dCas9-Tet1, two control groups were established: an untreated blank control and a group transfected with non-targeting sgRNA plus the dCas9-Tet1 plasmid. Transfections were performed using Lipofectamine™ 3000 (Thermo Fisher, L3000150, USA) according to the manufacturer's protocols (Haleem-Smith et al., 2005). Each well was transfected with 1 250 ng of sgRNA (evenly distributed across different combinations) and 1 250 ng of dCas9-Tet1 plasmid. After 6–8 h, transfection medium was replaced with complete medium, and cells were cultured for an additional 3 days to monitor growth and expression.

Decitabine treatment

Decitabine (5-aza-2'-deoxycytidine, 5-AZA-CdR) (Selleck, S1200, USA) was dissolved in 100% dimethyl sulfoxide (DMSO, Solarbio, D8371, China) to prepare a 10^5 μmol/L stock solution and diluted in complete culture medium to experimental concentrations of 10 and 20 μmol/L. Cells were seeded in 6-well plates and cultured for 24 h prior to treatment. Decitabine was applied at the indicated concentrations for 48 h. Cells were then collected using a cell scraper, a portion was lysed with TRIzol reagent for RNA extraction, while the remainder was snap-frozen in liquid nitrogen for DNA extraction. For methylation analysis, two primer pairs were designed for bisulfite sequencing, targeting regions containing 27 and 22 CpG sites, respectively (Supplementary Table S3).

RNA and DNA extraction

Cells were scraped from each well, resuspended in 1 mL of phosphate-buffered saline (PBS, Solarbio, P1020, China), pooled from replicate wells, and aliquoted equally into two centrifuge tubes. After centrifugation at 1 500 r/min for 2 min at 4°C, one pellet was snap-frozen in liquid nitrogen and stored at –80°C for whole-genome bisulfite sequencing (WGBS), while the second pellet was lysed with 1 mL of TRIzol reagent for total RNA extraction, following the manufacturer's protocols. Purified RNA was dissolved in 20 μL of water, and its concentration and quality were assessed. A 15 μL aliquot was reserved for RNA sequencing (RNA-seq) analysis, while the remainder was stored at –80°C. For DNA extraction, the phenol phase was washed with 1 mL of 0.1 mol/L sodium citrate solution (prepared in 10% alcohol) and dissolved in 20 μL of 8 mmol/L NaOH solution. DNA concentration was determined, and samples were stored at –80°C.

Reverse transcription quantitative PCR (RT-qPCR)

cDNA was synthesized from total RNA using a PrimeScript™ RT Reagent Kit with gDNA Eraser (Perfect Real Time, TAKARA, RR047A, Japan), according to the manufacturer's instructions. Primer sequences were designed using Primer v.5 (Supplementary Table S4). Amplification was performed using a 2× QuantiFast SYBR Green RT-qPCR Kit (Qiagen, 204156, Germany) on a Roche LightCycler®96 system. Each 20 μL reaction contained 10 μL of SYBR Green Master Mix, 1 μL of cDNA template (20 ng), 0.7 μL of forward and reverse primers, and 7.6 μL of DEPC-treated water. Melting curve analysis was performed to confirm product specificity. Relative gene expression was quantified using the $2^{-\Delta\Delta Ct}$ method based on Ct values of the internal reference gene (*β-actin*) and target gene (Livak & Schmittgen, 2001). Experiments were performed in triplicate with three independent biological replicates. Statistical analyses were conducted using GraphPad Prism v.9.5.1. Differences among experimental groups (dCas9-Tet1, dCas9-Tet1 Mix1, and dCas9-Tet1 Mix2) were assessed by one-way or two-way analysis of variance (ANOVA) followed by Dunnett's multiple comparisons test. Statistical significance thresholds were defined as follows: ns: Not significant; *: $P<0.05$; **: $P<0.01$; ***: $P<0.001$.

Kyoto Encyclopedia of Genes and Genomes (KEGG) pathway enrichment and protein-protein interaction (PPI) analysis

KEGG enrichment analysis was performed on genes significantly up-regulated ($P<0.01$, fold change≥2) following

treatment with 10 and 20 μmol/L decitabine. As *O. melastigma* is not currently supported in the Metascape database (https://metascape.org), differentially expressed genes (DEGs) were first mapped to their corresponding zebrafish orthologs using the Ensembl Genome Browser 113. Enrichment analysis of the converted gene set was then conducted in Metascape (Zhou et al., 2019). The KEGG enrichment analysis results shown in the Supplementary Figures are based on RNA-seq data, with enrichment performed using clusterProfiler (Wu et al., 2021; Yu et al., 2012) and calculated based on hypergeometric distribution.

Given the established roles of *fgf2* in cell proliferation (Dupree et al., 2006; Yu et al., 2016) and stem cell differentiation (Lotz et al., 2013), four pathways relevant to these processes were screened from the KEGG database: “Notch signaling pathway”, “Growth hormone synthesis, secretion, and action”, “Rap1 signaling pathway”, and “Signaling pathway regulating pluripotency of stem cells”. Genes involved in these pathways were submitted to the STRING database (https://string-db.org) (Szklarczyk et al., 2019), and a PPI network was generated using the *O. melastigma* protein reference set. Following removal of disconnected nodes, the core interaction network revealed FGF2 as a central hub interacting with downstream regulators such as FGFR, EGFR, and PDGFR.

Bisulfite sequencing PCR (BSP)

Genomic DNA was bisulfite-converted using a Vazyme EpiArt DNA Methylation Bisulfite Kit (Vazyme, EM102-01, China). PCR amplification of bisulfite-treated DNA was performed with primers designed via MethPrimer (Supplementary Table S3) using Vazyme 2× EpiArt HS Taq Master Mix (Dye Plus) (Vazyme, EM202, China). Amplified products were resolved by 1% agarose gel electrophoresis, and bands corresponding to the target fragments were excised, purified, and ligated into the pEAZY-T1 vector. Sanger sequencing was subsequently performed on the ligated products. Methylation status was analyzed using BiQ-Analyzer software (Bock et al., 2005).

RNA-seq and differential expression analysis

Total RNA was extracted from cells stored at –80°C using TRIzol reagent according to the manufacturer’s instructions. RNA quality and quantity were assessed using an RNA Nano 6000 Assay Kit with the Agilent Bioanalyzer 2100 system (Agilent Technologies, USA). Subsequently, RNA sequencing libraries were constructed using the NEB Next® Ultra RNA Library Prep Kit for Illumina® (E7530L, USA), following the NEBNext Ultra Directional RNA protocols. Sequencing was performed on the Illumina HiSeq2000 platform (Illumina, USA). Transcript abundance was quantified using RSEM v.1.2.4, which calculated FPKM (fragments per kilobase of exon per million mapped reads) values for each gene, and differential expression was analyzed using DESeq v.1.14.0 (Bioconductor v.2.14). After correction, genes with |log2 fold change|≥1.0 and P<0.01 were considered DEGs.

WGBS and data processing

Genomic DNA was isolated from snap-frozen cells using the CTAB method and sheared into 100–300 bp fragments by sonication. Fragmented DNA was ligated to sequencing adapters and subjected to bisulfite conversion using the EpiTech Bisulfite Kit (Qiagen, Germany). Converted libraries were sequenced on the Illumina NovaSeq X Plus platform (Illumina, USA). Clean reads were mapped to the *O. melastigma* reference genome using BSMAP software, allowing up to four mismatches per read (Xi & Li, 2009). Differentially methylated regions (DMRs) were identified using a sliding window approach with a window size of 200 bp and step size of 100 bp. Windows containing ≥5 GCs, an absolute methylation difference ≥0.25, and P≤0.05 were retained for CG-DMR detection (Akalin et al., 2012; Shao et al., 2014). Three biological replicates were included per treatment group.

Growth curve analysis

Cells were dissociated using trypsin-EDTA and resuspended in complete medium. After dilution, 100 μL of cell suspension was seeded into 96-well plates at approximately 2 000 cells per well across seven serial dilution groups. Following 4 h of incubation for adherence, medium was replaced with 100 μL of reduced-serum medium, followed by the addition of 10 μL of CCK-8 reagent (Yeasen, 40203ES, China). After an additional 4 h of incubation, absorbance at 450 nm was measured to construct a standard curve correlating optical density (OD) with cell number.

For experimental assays, cells were plated into 96-well plates under the following conditions: blank control, non-sgRNA-guided dCas9-Tet1 control, and two sgRNA-guided groups (dCas9-Tet1-Mix1 and dCas9-Tet1-Mix2). Seven replicate plates were prepared, each containing five replicate wells per group. After 24 h of incubation to allow attachment, one plate was processed to measure baseline OD using CCK-8, while the remaining cells were transfected with their respective plasmids. After 8 h, transfection medium was replaced with complete medium. One plate was harvested every 24 h to measure OD, and corresponding cell numbers were calculated using the standard curve. Growth curves were generated, and statistical analysis was conducted using two-way ANOVA followed by Dunnett’s multiple comparisons test to evaluate differences between experimental and control groups across days 1–7.

RESULTS

Molecular cloning and characterization of *tet1* in *O. melastigma*

The full-length *tet1* gene sequence of *O. melastigma*, retrieved from the NCBI database, spans 6 105 bp and encodes 2 034 amino acids. Two conserved domains were predicted: zf-CXXC and Tet_JBP (Supplementary Figure S1). Comparative sequence analysis across representative taxa—including *Branchiostoma floridae* (Cephalochordata), teleosts, amphibians, reptiles, birds, and mammals—revealed that *tet1* in teleosts formed a distinct phylogenetic clade, while mammals, birds, amphibians, and reptiles formed another cluster (Figure 1A). The *tet1* sequence of *O. melastigma* showed highest similarity to that of *Oryzias latipes*, indicating strong conservation within the genus (Figure 1A; Supplementary Figure S2). Domain organization analysis demonstrated widespread conservation of the zf-CXXC motif, and the Tet_JBP domain was restricted to a subset of taxa, and a Tet1 domain appeared in others (Figure 1A). Tertiary structure prediction further revealed that the *O. melastigma* Tet1 protein was structurally similar to the mouse TET1 homolog (Figure 1B; Supplementary Figure S3).

Next, *tet1* expression was systematically examined across adult tissues and throughout embryonic development in *O. melastigma*. RT-qPCR analysis showed pronounced tissue

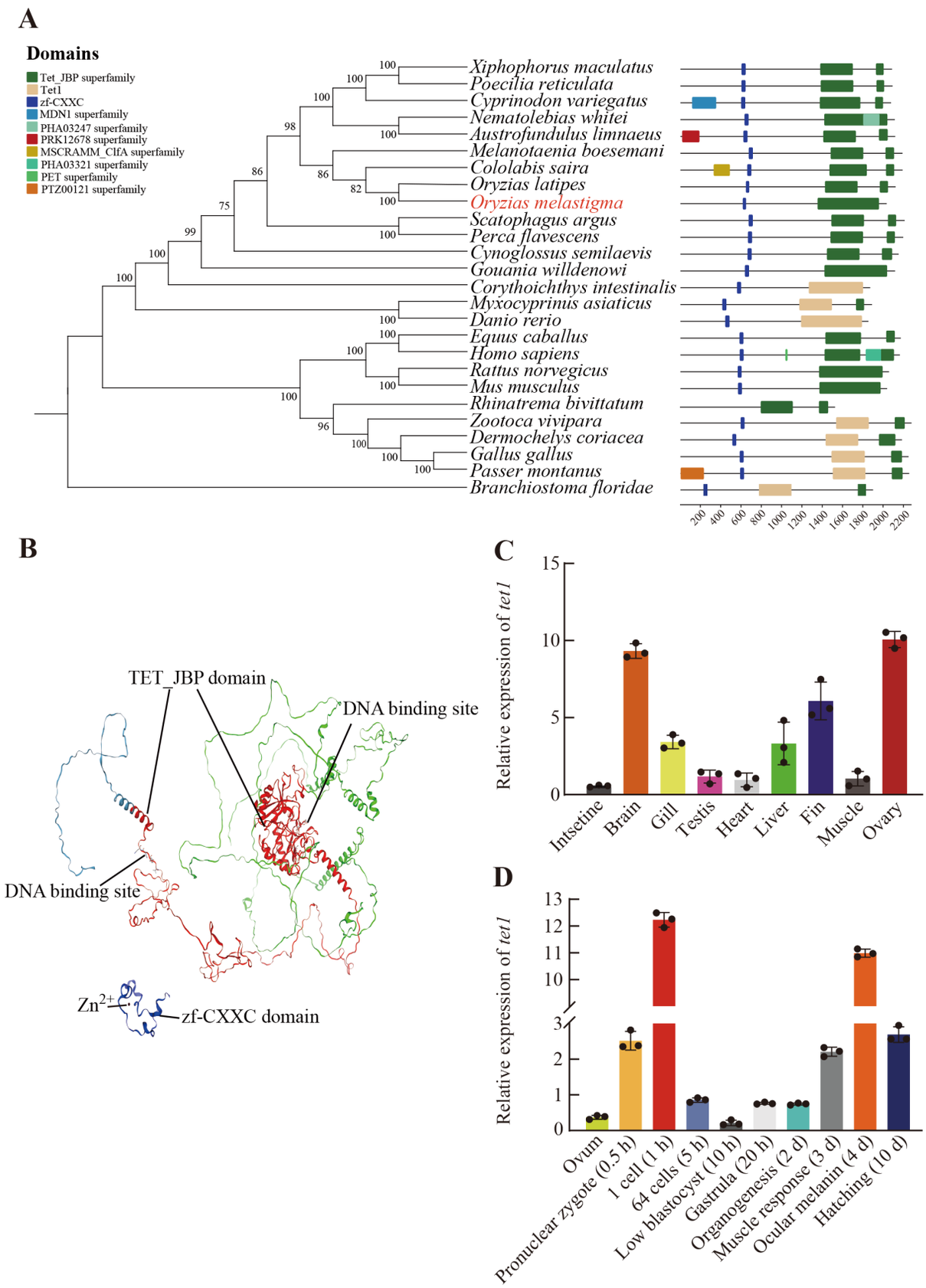

Figure 1 Molecular cloning and characterization of *tet1* in *O. melastigma*

A: Phylogenetic analysis of Tet1 amino acid sequences and domain characterization. Left panel shows phylogenetic tree based on neighbor-joining method, with node values representing percentage of bootstrap support based on 1 000 replicates. Right panel shows domain analysis, with different colored rectangles corresponding to distinct functional domains. B: Prediction of tertiary structure of Tet1 protein from *O. melastigma*. Dark blue region represents zf-CXXC domain, red region represents TET_JBP domain. C, D: Relative expression levels of *tet1* in different *O. melastigma* tissues (C) and different stages of embryonic development (D). Error bars represent mean±standard deviation (SD) (biological replicates *n*=3).

specificity, with highest transcript abundance detected in the ovary, followed by the brain and fin, while relatively low levels were detected in the intestine, testis, and heart (Figure 1C). During embryogenesis, *tet1* exhibited a dynamic and stage-dependent expression profile. Specifically, transcript levels peaked at the one-cell stage, progressively declined through the low blastocyst stage, increased sharply to a maximum at the ocular melanin stage, and subsequently decreased during later developmental stages (Figure 1D).

Identification of *fgf2* as a target gene of DNA methylation following decitabine treatment

Decitabine is a potent, broad-spectrum inhibitor of DNA methylation that replaces cytosine and covalently binds to DNA methyltransferases (DNMTs), irreversibly inhibiting their enzymatic activity. This compound has been widely employed in pharmacological research, molecular biology, and clinical oncology, particularly for reactivating tumor suppressor genes epigenetically silenced by promoter hypermethylation (Ramakrishnan et al., 2017; Qiu et al., 2025). To identify methylation-sensitive genes in *O. melastigma*, primary testis cells were exposed to 10 μmol/L or 20 μmol/L decitabine. Transcriptomic analysis revealed 1 907 and 2 020 genes were significantly up-regulated under the respective treatment conditions (Figure 2A; Supplementary Figure S4A, B), including *mafb*, *ihhb*, *egr3*, and *sox2*, which are involved in gene transcription, whereas genes associated with developmental regulation, such as *tgfb1*, *ebf1*, *ank1*, *ar*, and *sp8b*, were significantly down-regulated (Supplementary Data S1).

KEGG enrichment analysis revealed substantial overlap in pathway activation between both treatment groups, with the most enriched pathways including “ECM-receptor interaction”, “Protein digestion and absorption”, and “PI3K-Akt signaling pathway” (Supplementary Figure S4C, D). A total of 1 694 genes were up-regulated across both decitabine concentrations (Figure 2B). Functional enrichment of this overlapping gene set highlighted pathways related to energy metabolism and cell signaling, such as “Oxidative phosphorylation”, “Carbon metabolism”, “ECM-receptor interaction”, and “MAPK signaling pathway” (Figure 2C).

Among the shared targets, *fgf2* was identified as a candidate gene regulated by decitabine. This gene is a conserved regulator of cell proliferation, differentiation, and migration, acting through high-affinity binding to fibroblast growth factor receptors (FGFRs) (Nickle et al., 2024). In mammals, *fgf2* plays a critical role in organogenesis, including formation of the eyes, ears, heart, and synovial cartilage, and supports chondrocyte expansion during skeletal development (Krejci et al., 2007; Roddy et al., 2011; Yasuda et al., 1992; Yaylaoglu et al., 2005). In fish, high *fgf2* expression promotes germ cell proliferation, migration, and differentiation into spermatogonia or oogonia (Jin et al., 2023; Wong & Collodi, 2013). Epigenetically, *fgf2* has been identified as a potential biomarker for sarcopenia and is subject to regulation via H3K9me3 histone modifications and promoter DNA demethylation (Chaudhury et al., 2014; Li et al., 2024a). Analysis using MethPrimer (Li & Dahiya, 2002) identified a CpG island in the *fgf2* promoter region spanning –1 989 to –1 640 bp upstream of the *fgf2* transcription start site in *O. melastigma* (Figure 2D). Bisulfite sequencing revealed that decitabine treatment reduced the methylation level of this region from 85.72% to 73.06% at 10 μmol/L and to 68.78% at 20 μmol/L, corresponding to a maximal demethylation rate of 16.94% (Figure 2E; Supplementary Figure S4E). Concordantly, *fgf2* expression increased in a dose-dependent manner following decitabine exposure (Figure 2F, G).

Construction of CRISPR/dCas9-Tet1CD activation system and targeted epigenetic activation of *fgf2*

We constructed a CRISPR/dCas9-Tet1CD system for DNA demethylation editing in *O. melastigma*. The Tet1CD sequence (Ala1352 to Thr2034) including conserved Tet_JBP domain was fused with dCas9 (D10A and H840A) (Qi et al., 2013), controlled by the Ubc promoter, and a nuclear localization signal (NLS) was added (Figure 3A, B; Supplementary Figure S5A and Data S2). Five sgRNAs were designed to target distinct regions within the *fgf2* promoter, each driven by a separate U6 promoter (Figure 3A, B).

Transfection experiments were conducted using dCas9-Tet1 plasmid alone or in combination with individual sgRNAs or sgRNA pools. The results showed that compared with the control group consisting of untransfected cells, *tet1* overexpression was successfully achieved (Supplementary Figure S5B). Co-transfection with sgRNAs led to increased *fgf2* expression, with the strongest activation observed in groups co-transfected with three sgRNAs (sgRNA1+2+3, Mix1; 2.18-fold) or four sgRNAs (sgRNA2+3+4+5, Mix2; 2.41-fold) (Figure 3C).

BSP analysis indicated a significant reduction in methylation within the CpG island of the *fgf2* promoter in both Mix1 and Mix2 groups compared with the control and dCas9-Tet1-only groups (Figure 3D; Supplementary Figure S5C). WGBS analysis confirmed this demethylation effect, showing methylation levels of 99.87% in the control group and 98.12% in the dCas9-Tet1 only group, reduced to 77.15% and 81.47% in the Mix1 and Mix2 groups, respectively (Figure 3E).

Evaluation of off-target effects associated with CRISPR/dCas9-Tet1CD activation system

Off-target activity arising from nonspecific sgRNA binding remains a primary constraint of CRISPR/Cas9 platforms (Chen et al., 2019), necessitating rigorous assessment of editing specificity. To evaluate potential off-target effects of the CRISPR/dCas9-Tet1CD activation system, WGBS analysis was performed on control, dCas9-Tet1, Mix1, and Mix2 groups (n=3). On average, 21.757 Gb of high-quality methylome data were obtained per sample, with an average alignment rate of 71.58% to the reference genome and an average sequencing depth of 20.589×. CG methylation accounted for 73.922% of total methylated cytosines (mCs) (Supplementary Table S5).

CpG methylation was further analyzed across genomic features, including exons, 5' untranslated regions (UTRs), introns, promoters, and 3' UTRs (Supplementary Figure S6A and Table S6). Methylation levels were consistently low near the transcript start sites (TSSs), and global methylation patterns in editing groups resembled those of the control group (Figure 4A, B). Notably, global chromosomal methylation remained similar in Mix1 and Mix2 groups compared to the control, whereas a modest decrease was observed in the dCas9-Tet1 only group (Figure 4B; Supplementary Data S3).

Subsequent analysis identified a total of 250 DMRs (152 hypermethylated and 98 hypomethylated) between the Mix1 and control groups, and 75 DMRs (31 hypermethylated and 44 hypomethylated) between the Mix2 and control groups (Figure 4C). In both comparison groups, DMRs were

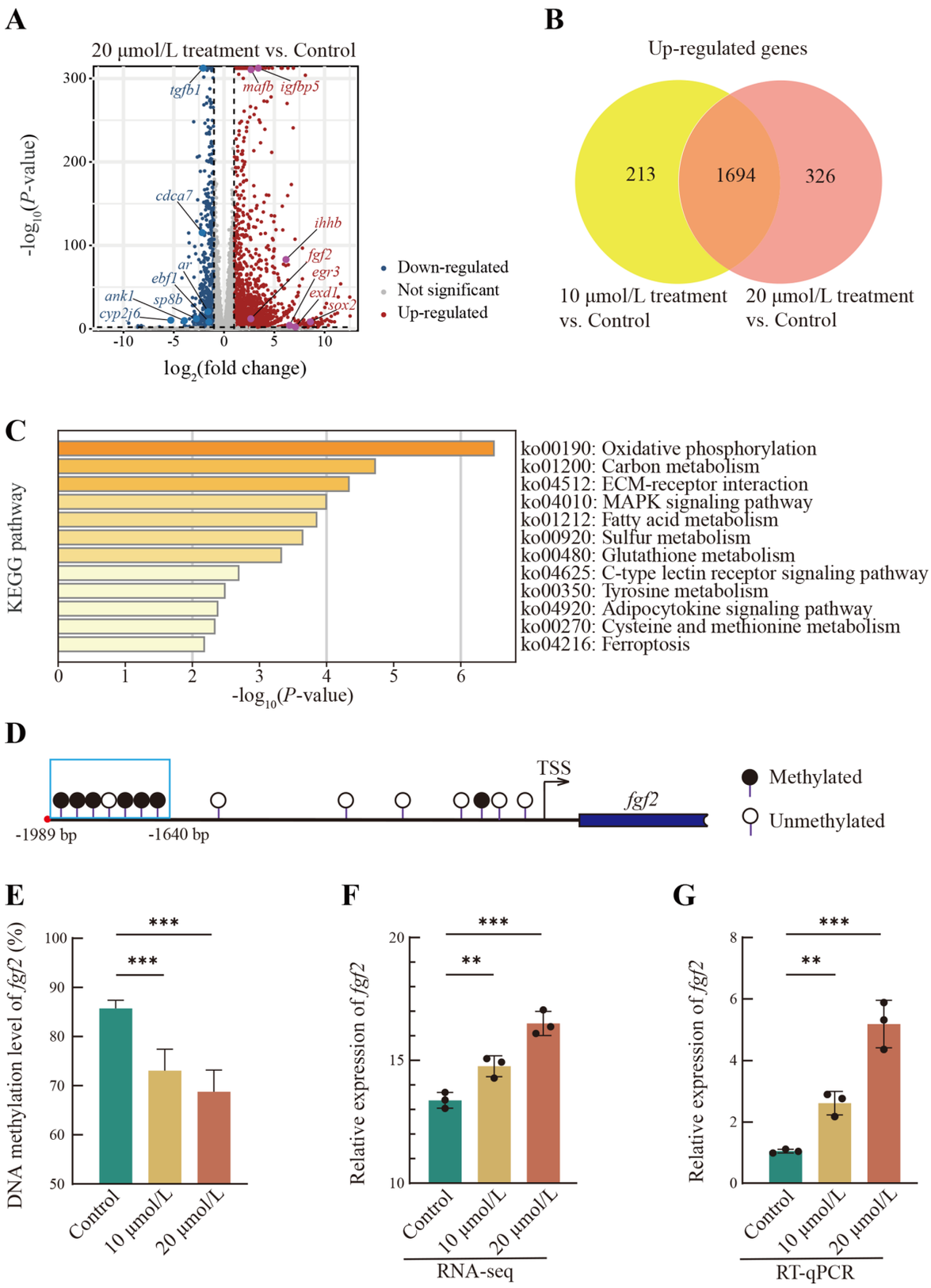

Figure 2 Effects of decitabine treatment on gene expression and DNA methylation in *O. melastigma* primary testis cells

A: Volcano plot showing differentially expressed genes (DEGs) following 20 μmol/L decitabine treatment. Dark blue and red indicate significantly down- and up-regulated DEGs, respectively. B: Venn diagram displaying overlap of up-regulated genes after treatment with 10 μmol/L and 20 μmol/L decitabine. C: KEGG pathway enrichment analysis of up-regulated DEGs (fold change≥2, P<0.01) from both treatment groups. D: Schematic representation of DNA methylation in the *fgf2* promoter CpG island following decitabine exposure. E: Bisulfite sequencing PCR (BSP) results showing average methylation rates based on 10 replicates per group. F, G: Expression levels of *fgf2* assessed by RNA-seq (F) and validated by RT-qPCR (G). Statistical significance was determined by one-way ANOVA followed by Dunnett's multiple comparisons test versus control. Error bars represent mean±SD (n=3). *: P<0.05; **: P<0.01; ***: P<0.001.

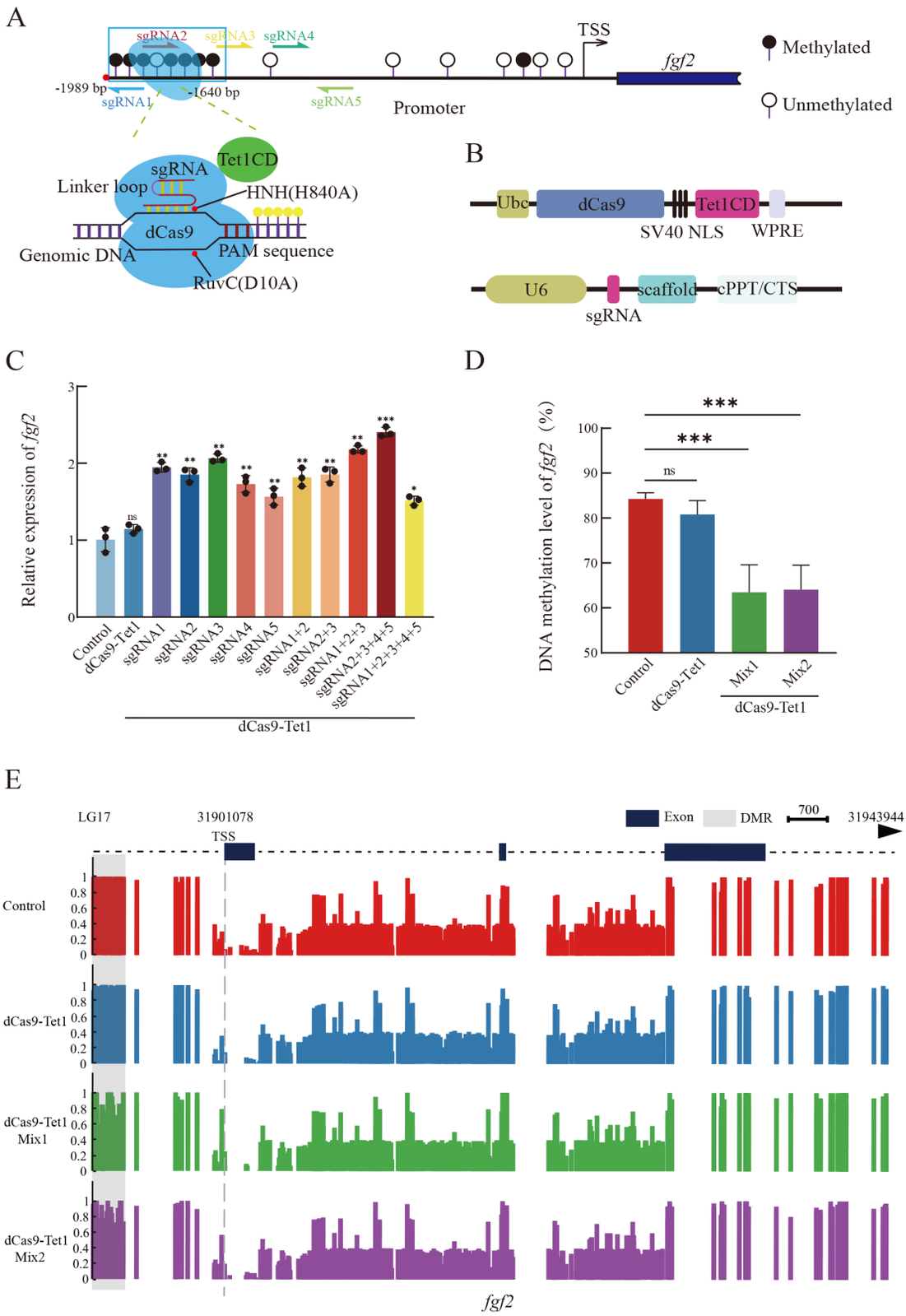

Figure 3 Design and construction of CRISPR/dCas9-Tet1CD activation system targeting *fgf2*

A: Schematic representation of the CRISPR/dCas9-Tet1CD system targeting the *fgf2* promoter region. Blue box denotes *fgf2* promoter CpG island, colored arrows indicate relative positions of sgRNAs, and green dashed box represents fusion plasmid of dCas9-Tet1 and sgRNAs targeting specific DNA sequences. B: Upper panel shows the structural layout of the dCas9-Tet1 fusion plasmid; lower panel illustrates the configuration of the sgRNA expression vector. C: Expression levels of *fgf2* following transfection with dCas9-Tet1 alone or in combination with individual sgRNAs or sgRNA pools. D: DNA methylation levels of the *fgf2* promoter CpG island, determined by bisulfite sequencing PCR (BSP) across 10 replicates per group. E: DNA methylation profile of *fgf2*; shaded area represents differentially methylated region (DMR). Statistical analysis was performed using one-way ANOVA followed by Dunnett's multiple comparisons test versus control. Error bars represent mean±SD (n=3). *: P<0.05; **: P<0.01; ***: P<0.001; ns: Not significant.

consistently enriched in eight hypomethylated DMR-associated genes (*rxfp3, gad2, cerk, mfsd2b, snx9, ptbp2, fgf2,* and *LOC118598063*) and five hypermethylated DMR-associated genes (*cd163l1, fbxw8, rab28, gpr158,* and *LOC118599107*) (Supplementary Figure S6B). To determine whether these DMRs influenced gene expression, DEGs overlapping with hypomethylated DMRs were identified. Seven genes (*slx4ip*, *tet2*, *fgf2*, *dffa*, *rftn1*, *mast4*, and *si:dkey-122a22.2*) exhibited concurrent hypomethylation and transcriptional up-regulation in the dCas9-Tet1 and Mix1 groups, while only two genes (*fgf2* and *LOC112162194*) showed similar hypomethylation-associated up-regulation in cells co-transfected with dCas9-Tet1 and Mix2 compared to the control group (Figure 4D; Supplementary Data S4). Importantly, there were no off-target sites for *fgf2* sgRNAs in the other seven genes (*slx4ip*, *tet2*, *dffa*, *rftn1*, *mast4*, *si:dkey-122a22.2*, and LOC112162194) analyzed by the CRISPOR (Concordet & Haeussler, 2018) and CCTop (Stemmer et al., 2015) tools. We also analyzed the methylation level and the expression level change of predicted off-target genes, including *znf423*, *eif2a*, *bbs12*, and *samhd1* (Supplementary Data S5). Both the methylation level and the gene expression level were not significantly changed (Figure 4E; Supplementary Figure S6C). The above results indicate that our CRISPR/dCas9-Tet1CD activation system has low off-target effects.

Epigenetic activation of *fgf2* alters expression of growth-related genes

To examine transcriptional changes induced by *fgf2* demethylation, transcriptome profiles of edited cells were compared with controls. In total, 1 267 and 767 genes were up-regulated, while 302 and 151 genes were down-regulated in the two edited groups, respectively (Figures 4D, 5A, B). Up-regulated transcripts included *bmp2*, *sox13*, *ets1*, and *trim27*, while down-regulated transcripts included *egr1*, *dusp2*, *junb*, and *fos* (Figure 5A, B; Supplementary Data S6).

KEGG enrichment analysis of DEGs revealed significant involvement of the “MAPK signaling pathway”, “Ras signaling pathway”, and “Parathyroid hormone synthesis, secretion and action” (Supplementary Figure S7A, B). Genes involved in “signaling pathway regulating pluripotency of stem cells” were also up-regulated (Figure 5C), alongside pathways regulating proliferation and differentiation, including the “Notch signaling pathway”, “Growth hormone synthesis, secretion, and action”, and “Rap1 signaling pathway” (Supplementary Figure S8A–C). Notably, *wnt9a* and *hras* expression increased following *fgf2* activation (Figure 5D), consistent with previous reports of their roles as key regulators of cell proliferation (Rajalingam et al., 2007; Richter et al., 2018). These findings suggest that epigenetic activation of *fgf2* may affect cell growth and differentiation through multiple signaling pathways. Additional signaling-related DEGs, such as *notch3*, *stat1*, *junb*, and *mapk1*, were also affected (Supplementary Figure S8D).

Next, PPI analysis of growth-related DEGs (P<0.01) identified a network comprising 36 nodes and 82 edges after removal of unconnected nodes (Figure 5E). Core components included known *fgf2*-interacting receptors such as *fgfr4* (Huang et al., 2023), *pdgfrβ* (Zhao et al., 2021), *pdgfrα* (Nissen et al., 2007), and *egfr* (Cai et al., 2020), suggesting that epigenetic activation of *fgf2* modulates growth-related signaling pathways.

Sustained induction of *fgf2* expression and enhanced cell proliferation by CRISPR/dCas9-Tet1CD activation

DNA methylation is a key epigenetic modification that governs gene regulation and can be stably maintained through cell divisions and across generations (Guo et al., 2025; Takahashi et al., 2023). This stability enables long-lasting transcriptional modulation through methylation editing. Following validation of the efficacy and specificity of the CRISPR/dCas9-Tet1CD activation system, the durability of *fgf2* transcriptional activation was evaluated over 9 days post-transfection. Results showed that *fgf2* expression remained significantly elevated relative to the control across all time points (Figure 6A). Notably, dCas9 expression peaked at day 3 and declined thereafter, becoming undetectable by day 9 (Figure 6B), indicating that *fgf2* activation persisted even without nascent dCas9-Tet1 expression.

Given that *fgf2* is a known regulator of cell proliferation (Nishida et al., 2011), the functional impact of its activation was assessed in a cell growth assay. Notably, no significant difference in cell density was observed between the edited and control groups during the initial 4 days. However, during the subsequent exponential phase, the edited group exhibited a higher proliferation rate than the control, resulting in significantly increased cell density (Figure 6C). These results demonstrate that CRISPR/dCas9-Tet1CD-mediated epigenetic activation of *fgf2* elicits sustained gene expression and promotes enhanced cell growth.

DISCUSSION

This study identified the DNA demethylase Tet1 from marine medaka and established a CRISPR/dCas9-Tet1CD-based epigenetic activation system by fusing Tet1CD to dCas9. Using sgRNAs targeting the *fgf2* promoter region, this programmable system enabled targeted DNA demethylation and robust up-regulation of *fgf2* transcription. Furthermore, WGBS analysis confirmed minimal off-target effects. Notably, *fgf2* up-regulation persisted beyond the detectable presence of dCas9, indicating sustained transcriptional activation following transient editing. Growth assays further demonstrated that *fgf2* activation enhanced the proliferative capacity of primary testis cells. These findings provide a more complete framework for epigenetic editing in marine teleosts, with implications for functional studies, aquaculture, and conservation biology.

DNA methylation represents a key epigenetic mechanism that mediates genome-environment interactions (Johnston et al., 2024; Zhang et al., 2025). The present study identified a functional Tet1 ortholog in marine medaka, characterized by evolutionarily conserved domains. All examined species harbored a zf-CXXC domain capable of recognizing non-methylated CpG sequences, along with either a Tet1 or Tet_JBP domain (Figure 1A). Although the Tet_JBP family originated from bacterial or bacteriophage lineages, only in eukaryotes have Tet_JBP and Tet1 been established as homologs essential for epigenetic regulation (Burke et al., 2021; Iyer et al., 2009). In marine medaka, *tet1* expression exhibited tissue specificity and developmental stage dependence, emphasizing its involvement in DNA demethylation during early ontogeny, particularly embryogenesis (Figure 1C, D). In Japanese medaka, embryos undergo two rounds of reprogramming to a totipotent state—during the blastocyst stage and shortly after fertilization—to support developmental progression (Wang &

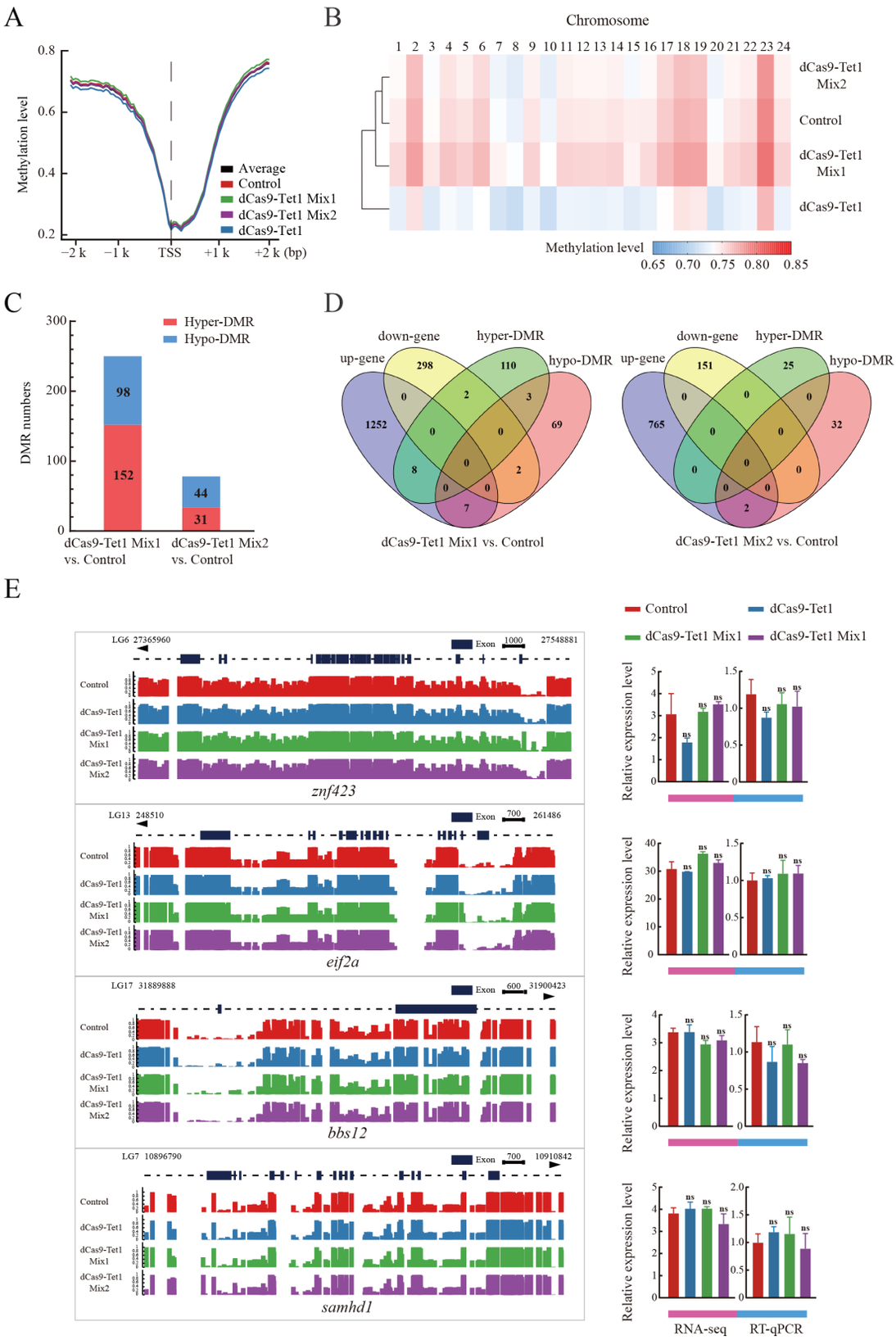

Figure 4 Evaluation of off-target effects following CRISPR/dCas9-Tet1CD-mediated activation

A: DNA methylation profile surrounding transcription start sites (TSSs) in CRISPR/dCas9-Tet1CD-edited and control groups. Dashed gray line denotes TSS position. B: Chromosome-wise average methylation levels across treatment groups. C: Number of DMRs between Mix1 vs. control and Mix2 vs. control comparisons, with counts of hypermethylated (Hyper) and hypomethylated (Hypo) DMRs indicated. D: Venn diagram showing overlap between DMR-related genes and DEGs for Mix1 vs. control (left) and Mix2 vs. control (right), including up-regulated genes, down-regulated genes, and genes associated with hyper- or hypomethylated DMRs. E: Methylation levels (left) and gene expression (right) of predicted off-target genes. Statistical significance was determined by one-way ANOVA followed by Dunnett's multiple comparisons test versus control. Error bars represent mean±SD (n=3). *: P<0.05; **: P<0.01; ***: P<0.001; ns: Not significant.

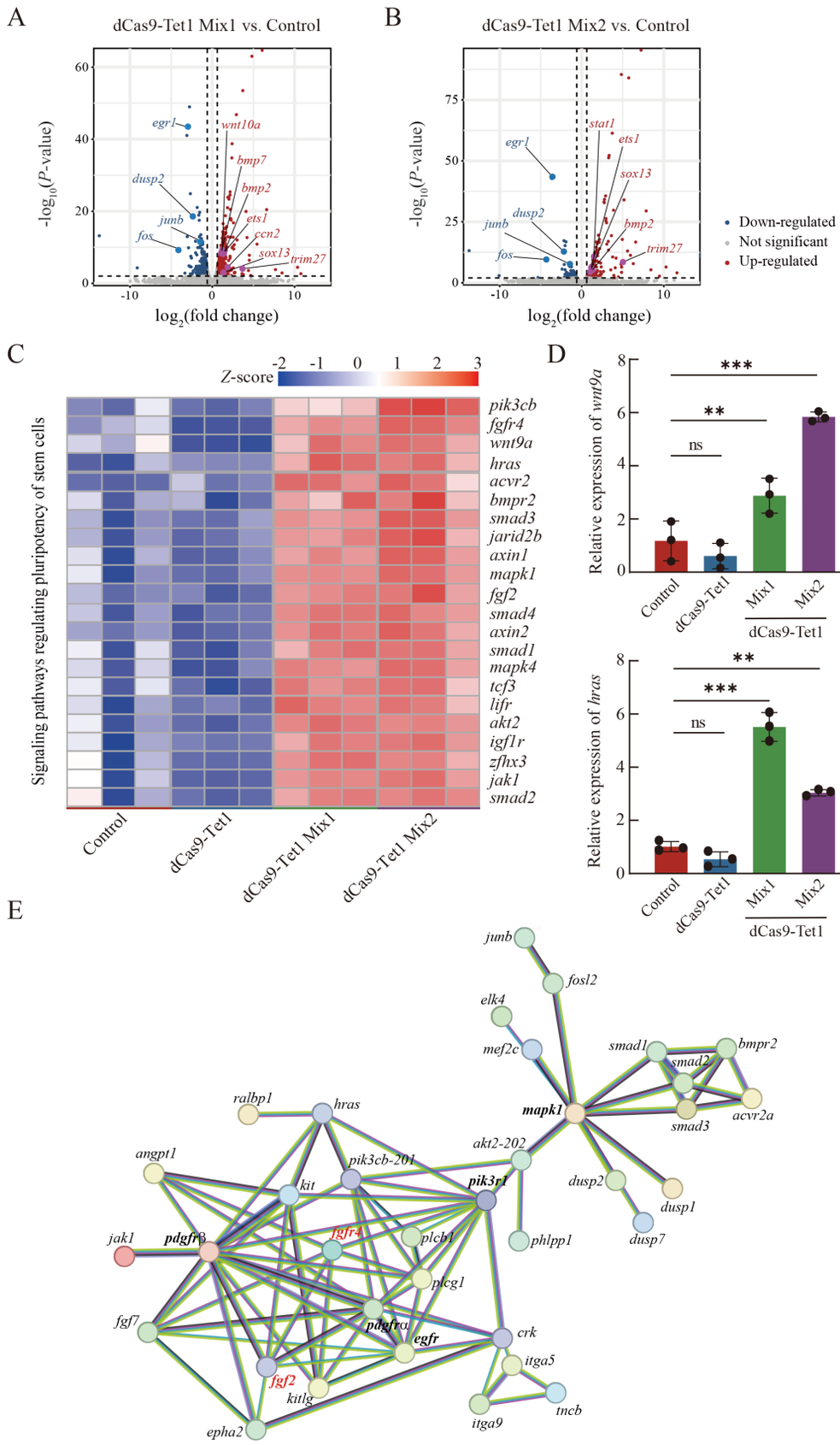

Figure 5 Transcriptomic analysis of signaling pathways and genes following epigenetic activation of *fgf2*

A, B: Volcano plot illustrating DEGs in dCas9-Tet1 Mix1 and Mix2 groups. Dark blue and red represent down-regulated and up-regulated genes, respectively. C: Heatmap of genes involved in proliferation and differentiation-related pathways downstream of *fgf2* in dCas9-Tet1 Mix1 and Mix2 groups. D: RT-qPCR validation of key proliferation and differentiation genes shown in the heatmap. E: Protein-protein interaction (PPI) network showing differentially abundant signature (DAS) genes (fold change≥1.5, P<0.01). Statistical significance was determined by one-way ANOVA followed by Dunnett's multiple comparisons test versus control. Error bars represent mean±SD (n=3). *: P<0.05; **: P<0.01; ***: P<0.001.

Bhandari, 2020a, 2020b). However, the methylation dynamics governing these transitions and their phenotypic consequences remain insufficiently characterized (Wang & Bhandari, 2020a, 2020b). Further investigation into the regulation of *tet1* and DNA methylation during medaka embryonic development is needed.

Targeted manipulation of DNA methylation has emerged as a promising approach across biomedical and biotechnological domains, particularly in the context of disease intervention. Inhibitors such as decitabine has been instrumental in studying the regulation of DNA methylation. In the current study, decitabine application enabled the identification of critical downstream targets, including *fgf2* and transcription factors such as *mafb*, *egr3*, and *sox2* (Figure 2A; Supplementary Figure S4A). These loci have been previously implicated in DNA methylation-dependent regulatory networks, reinforcing the importance of this epigenetic mark in transcriptional control (Chaudhury et al., 2014; Cyphert et al., 2019; Hu et al., 2017; Li et al., 2024a; Lu et al., 2013; Zhao et al., 2024). However, global DNA methylation induced by small-molecule inhibitors often lacks specificity, with off-target alterations across the epigenome.

To overcome the limitations of global demethylation approaches, recent advances in CRISPR/dCas9-based epigenetic editing have enabled site-specific modification of methylation without introducing genotoxic damage. The epigenetic editing, which is achieved by fusing DNA methyltransferases or demethylases to the dCas9 protein, allows for precise and targeted regulation of DNA methylation, then regulating gene expression (Choudhury et al., 2016; Qian & Liu, 2024). The CRISPR/dCas9-Tet1CD activation system developed and applied in marine medaka, along with comparable systems in other teleosts, highlights the feasibility of programmable epigenome editing in non-mammalian models (Fukushima et al., 2019; Liang et al., 2023). Unlike conventional CRISPR/Cas9 editing, which induces double-strand breaks to drive mutagenesis, dCas9-based approaches avoid DNA cleavage and minimize damage response pathways related genes, such as *TP53*, thereby reducing cell cycle arrest, apoptosis, and tumorigenesis (Álvarez et al., 2022). Cleavage-dependent editing is also limited by off-target effects that may trigger chromosomal rearrangement, gene silencing, or unintended perturbations of regulatory circuits, significantly limiting clinical translatability (Sander & Joung, 2014). In contrast to Cas9, the inactivated Cas9 protein loses the ability to cut DNA sequences, which reduces nonspecific binding and off-target to a certain extent. Tsai et al. used dCas9 to bind to a specific FokI nickase domain, which can cause DNA cleavage at a specific site, thereby reducing nonspecific binding and off-target (Tsai et al., 2014). When dCas9 was combined with single-stranded annealing protein (SSAP), it exhibited higher editing accuracy but lower editing efficiency in cell experiments (Wang et al., 2022a). Here, we provide a feasible strategy for up-regulation of endogenous genes in marine medaka. Upon transfected the CRISPR/dCas9-Tet1CD activation system, the expression level of *fgf2* increased, with a maximum of 2.41-fold (Figure 3C). Our system leverages DNA demethylation to activate gene expression without cutting DNA, rendering it a safer alternative. In addition, the results of WGBS analysis showed that although there are 250 and 75 DMRs were detected in the mix1 and mix2 treatments, respectively (Figure 4C), the presence of DMRs is normal because methylation changes can also occur due to gene activation, inhibition, or environmental factors (Mojica & Kültz, 2022). In conjunction with RNA-seq data, only 8 genes had reduced methylation levels accompanied by increased expression (Figure 4D). Excluding the target gene *fgf2*, the remaining seven genes lacked binding sites for our designed sgRNA, and no reduction in methylation and increased gene expression was observed in the predicted off-target genes (Figure 4E; Supplementary Figure S6C).

Extensive research has demonstrated the utility of dCas9 fused to various transcriptional regulators to modulate gene expression. Fusions with repressors such as KRAB or activators such as VP64 have been employed to silence or enhance transcription at targeted loci (Gilbert et al., 2013; Roy Choudhury et al., 2023). Epigenetic repression has also been achieved by fusing dCas9 to DNA methyltransferases such as DNMT3A. For instance, Vojta et al. (2016) constructed a dCas9-DNMT3A fusion protein capable of inducing promoter methylation at the *il6st* and *bach* gene loci, thereby suppressing their expression (Vojta et al., 2016). Using a similar strategy, targeted methylation with *dnmt3a* in Chinese tongue sole led to successful down-regulation of *emx2* expression. In terms of activation, transcriptional enhancement has been attempted by fusing dCas9 to potent activator domains such as VP64 and P65. Gilbert et al. fused dCas9 with VP64 protein and effectively activated the expression of Gal4UAS-GFP, but the system had limited effect on improving gene expression levels (Gilbert et al., 2013). Consequently, Lin et al. (2015) fused the highly active VP64-P65-RTA domain with dCas9 protein to construct the dCas9-VPR activation system. Regardless of whether it is the dCas9-VP64 or dCas9-VPR system, transcriptional activation ceases once the action of the activator ceases. In contrast, epigenetic editing enables durable gene activation by establishing heritable chromatin states. Chavez et al. (2015) proposed that epigenetic modulation may yield more stable transcriptional outcomes than direct activator fusions. Supporting this, Zhang et al. (2024b) showed that although expression of a PPAD-dCas9 fusion plasmid declined by day 10 after transfection, elevated levels of histone citrullination and sustained mRNA expression of the corresponding target gene persisted beyond this point. Consistently, the CRISPR/dCas9-Tet1CD system used in this study maintained overexpression of the target gene even in the absence of dCas9 protein expression (day 9) (Figure 6A, B), indicating prolonged epigenetic activation. This extended duration underscores a key advantage of the system. However, DNA methylation status was only assessed for 9 days, and the long-term stability of induced gene expression requires further investigation. Moreover, *in vivo* validation of CRISPR/dCas9-Tet1CD system efficacy in teleosts remains an important next step.

Successful gene editing relies heavily on the rational design of sgRNAs (Gao, 2021), as editing efficiency is directly influenced by the frequency of double-strand DNA breaks induced by Cas9. Poorly optimized sgRNAs can impede targeting precision and compromise editing outcomes. In this study, five sgRNAs were designed to target the *fgf2* promoter, with sgRNA1, sgRNA2, and sgRNA3—located progressively upstream of the TSS—showing higher editing efficiency than sgRNA4 and sgRNA5, which lie closer to the TSS (Figure 3A–C). While previous studies have shown that the distance between the sgRNA target sequence and TSS affects epigenetic editing efficiency (Larson et al., 2013), the

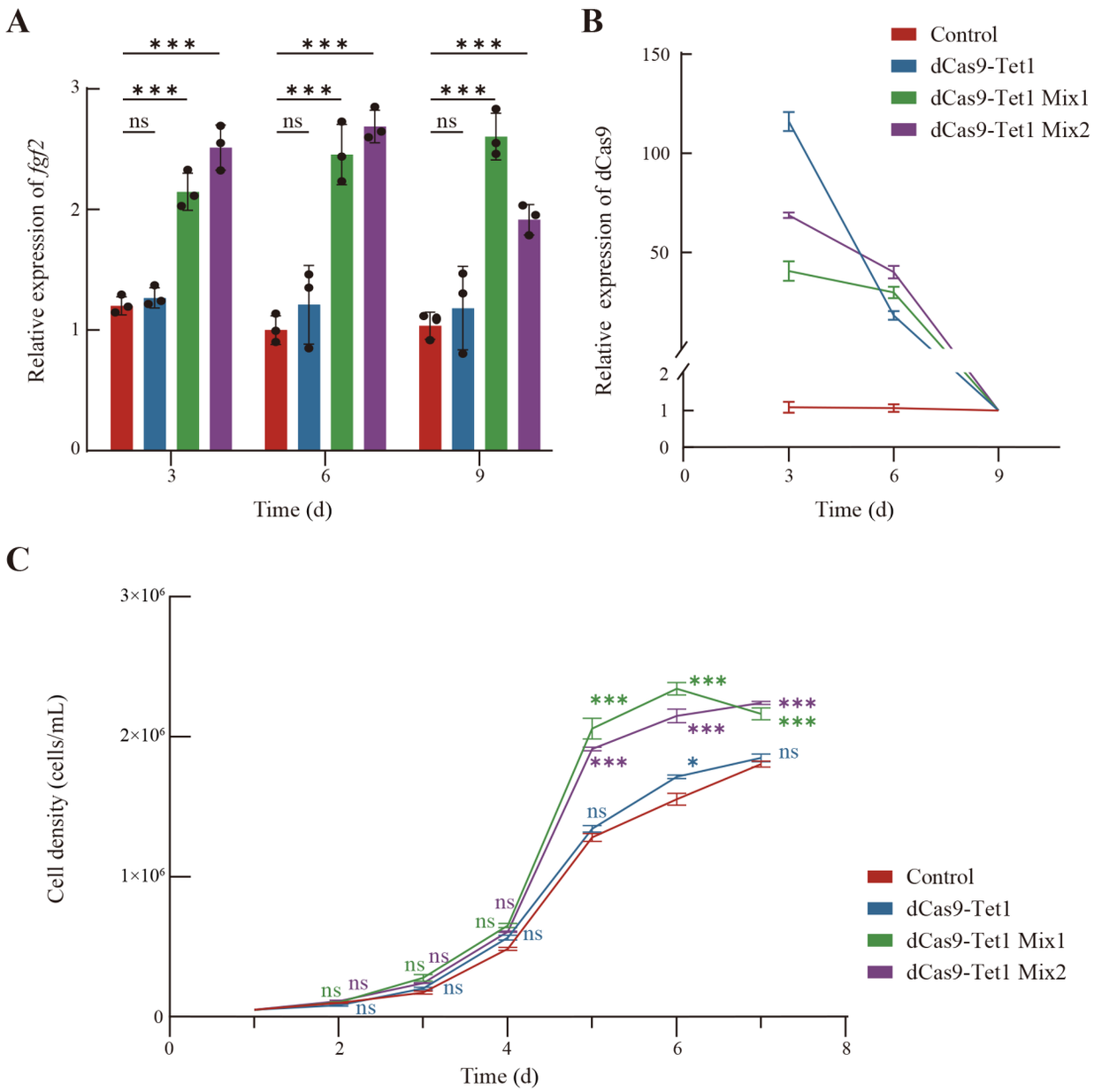

Figure 6 Sustained *fgf2* expression and enhanced cell proliferation induced by CRISPR/dCas9-Tet1CD activation

A, B: Cells from control and treatment groups were passaged every 3 days, and expression levels of *fgf2* and dCas9 were measured following each passage. In panel B, the y-axis represents dCas9 expression in each treatment group compared to control. C: Growth curves of primary testis cells after transfection with dCas9-Tet1, dCas9-Tet1-Mix1, and dCas9-Tet1-Mix2 constructs compared to control. No significant differences were observed between experimental and control groups during days 1 to 4. Statistical significance was determined by two-way ANOVA followed by Dunnett's multiple comparisons test versus control. Error bars represent mean±SD (n=3). *: P<0.05; ***: P<0.001; ns: Not significant.

present data revealed that all sgRNAs exerted comparable effects on gene expression (Figure 3C). This outcome may be attributed to the proximity of all sgRNA targets to the CpG island within the *fgf2* promoter region, where methylation changes likely play a more crucial role. Whether dCas9-Tet1 recruits additional transcription factors to regulate gene expression requires further investigation. Moreover, whether this system functions effectively at promoters lacking CpG islands needs to be verified in subsequent studies. Accumulating evidence suggests that the use of paired sgRNAs significantly improves editing efficiency compared to sgRNA strategies (Tang et al., 2018), potentially by altering local chromatin architecture and facilitating synergistic effects at adjacent sites (Vu et al., 2021). Surprisingly, even inefficient sgRNAs can augment activity when used in combination by modifying the chromosomal context (Kuscu et al., 2014). Consistent with these findings, combinatorial sgRNA use in this study yielded a maximal 2.41-fold increase in editing efficiency. Different combinations also produced consistent outcomes in regulating DNA methylation and gene expression. However, inclusion of inefficient sgRNAs (sgRNA4 and sgRNA5) in the optimal mix (Mix1) diminished overall efficiency, suggesting that a 3–4 sgRNA strategy may be optimal (Figure 3C, D). Nevertheless, despite these advances, further work is required to define generalizable principles for sgRNA selection in epigenetic editing platforms.

To further elucidate the regulatory impact of *fgf2*, KEGG pathway enrichment analysis was conducted following epigenetic activation of the locus. Prior research has demonstrated that FGF2 promotes gonadal granulosa cell proliferation by inhibiting Hippo signaling and activating *yap* expression, while also playing a key role in primordial germ cell reprogramming, maintenance of embryonic stem cells, and stabilization of fetal gonadal architecture (Cheng et al., 2024; Choi et al., 2018; Yu et al., 2016). Based on these known functions, attention was directed toward four KEGG pathways involved in cell proliferation and differentiation, including regulation of stem cell pluripotency, Rap1 signaling, Notch signaling, and growth hormone synthesis, secretion, and action (Figure 5C; Supplementary Figure S8A–C). PPI mapping revealed that *fgf2* not only interacts with canonical FGF receptors (FGFR1–4) but also with multiple tyrosine kinase receptors, including PDGFR, EGFR, and KIT (Figure 5E). These interactions influence the expression of downstream effectors such as MAPK1 and PIK3, suggesting a broader regulatory role of *fgf2*. This is consistent with earlier findings that FGF signaling involves cross-coordination among MAPK, PI3K/AKT, transcription activators (STAT), WNT, and TGF-β pathways to modulate diverse cellular outcomes (Mossahebi-Mohammadi et al., 2020). Among these, MAPK-related kinases are particularly effective at activating downstream genes that regulate proliferation, differentiation, apoptosis, and stress responses (Sulzmaier & Ramos, 2013). In addition to the up-regulation of *stat1* and *wnt9*, genes associated with placental and bone formation (*junb*), neural crest cell migration (*jarid2b*), and cellular proliferation and apoptosis (*hras*, *notch3*) also exhibited significant transcriptional changes. These findings underscore the complex and multifaceted role of *fgf2*, highlighting its potential as a key regulator in developmental and regenerative contexts.

Collectively, this study successfully established a CRISPR/dCas9-based epigenetic editing technique for *O. melastigma*, enabling precise gene activation through epigenetic reprogramming. This system provides a robust tool for studying DNA methylation dynamics and their phenotypic consequences. In addition to advancing fundamental understanding of epigenetic regulation in teleost development, this approach holds promise for the development of novel epigenome-informed therapeutic and aquaculture strategies.

DATA AVAILABILITY

Data are contained within the article. RNA-seq and WGBS data were submitted to the NCBI database (BioProjectID PRJNA1212316), Genome Sequence Archive (https://ngdc.cncb.ac.cn/gsa; accession number PRJCA039718), and Science Data Bank (https://www.scidb.cn/en; doi: 10.57760/sciencedb.24703). All data that support the findings of this study are available from the corresponding author upon reasonable request.

SUPPLEMENTARY DATA

Supplementary data to this article can be found online.

COMPETING INTERESTS

The authors declare that they have no competing interests.

AUTHORS' CONTRIBUTIONS

L.L.: Original Draft, Data Curation, Validation, Methodology, Visualization, Formal analysis, Writing; J.J.Z.: Validation, Visualization, Methodology, Resources. B.H.L.: Data Curation, Formal analysis. S.D.: Data Curation, Formal analysis. Y.Q.Z.: Conceptualization, Supervision. Y.Y.: Conceptualization, Supervision. C.L.: Conceptualization, Supervision. C.C.D.: Validation, Supervision. Y.B.H.: Resources, Supervision. Q.W.: Funding acquisition. C.W.S. and H.Y.W.: Writing, review & editing Conceptualization, Supervision, Investigation, Project administration, Funding acquisition, Resource.

REFERENCES

Ahmad M. 2023. Plant breeding advancements with "CRISPR-Cas" genome editing technologies will assist future food security. *Frontiers in Plant Science*, **14**: 1133036.

Akalin A, Kormaksson M, Li S, et al. 2012. methylKit: a comprehensive R package for the analysis of genome-wide DNA methylation profiles. *Genome Biology*, **13**(10): R87.

Álvarez MM, Biayna J, Supek F. 2022. TP53-dependent toxicity of CRISPR/Cas9 cuts is differential across genomic loci and can confound genetic screening. *Nature Communications*, **13**(1): 4520.

Bailey TL, Johnson J, Grant CE, et al. 2015. The MEME suite. *Nucleic Acids Research*, **43**(W1): W39–W49.

Bock C, Reither S, Mikeska T, et al. 2005. BiQ Analyzer: visualization and quality control for DNA methylation data from bisulfite sequencing. *Bioinformatics*, **21**(21): 4067–4068.

Burke EJ, Rodda SS, Lund SR, et al. 2021. Phage-encoded ten-eleven translocation dioxygenase (TET) is active in C5-cytosine hypermodification in DNA. *Proceedings of the National Academy of Sciences of the United States of America*, **118**(26): e2026742118.

Cai JD, Huang JN, Wang WL, et al. 2020. miR-124-3p regulates FGF2-EGFR pathway to overcome pemetrexed resistance in lung adenocarcinoma cells by targeting MGAT5. *Cancer Management and Research*, **12**: 11597–11609.

Cappelluti MA, Mollica Poeta V, Valsoni S, et al. 2024. Durable and efficient gene silencing in vivo by hit-and-run epigenome editing. *Nature*, **627**(8003): 416–423.

Chae K, Overcash JM, Dawson C, et al. 2023. CRISPR-based gene editing of non-homologous end joining factors biases DNA repair pathway choice toward single-strand annealing in *Aedes aegypti*. *Current Research in Biotechnology*, **5**: 100133.

Chaudhury S, Aurbach EL, Sharma V, et al. 2014. FGF2 is a target and a trigger of epigenetic mechanisms associated with differences in emotionality: partnership with H3K9me3. *Proceedings of the National Academy of Sciences of the United States of America*, **111**(32): 11834–11839.

Chavez A, Scheiman J, Vora S, et al. 2015. Highly efficient Cas9-mediated transcriptional programming. *Nature Methods*, **12**(4): 326–328.

Chen MJ, Mao AW, Xu M, et al. 2019. CRISPR-Cas9 for cancer therapy: opportunities and challenges. *Cancer Letters*, **447**: 48–55.

Cheng FY, Wang JY, Wang RL, et al. 2024. FGF2 promotes the proliferation of injured granulosa cells in premature ovarian failure via Hippo-YAP signaling pathway. *Molecular and Cellular Endocrinology*, **589**: 112248.

Choi KH, Lee DK, Oh JN, et al. 2018. FGF2 signaling plays an important role in maintaining pluripotent state of pig embryonic germ cells. *Cellular Reprogramming*, **20**(5): 301–311.

Choudhury SR, Cui Y, Lubecka K, et al. 2016. CRISPR-dCas9 mediated TET1 targeting for selective DNA demethylation at BRCA1 promoter. *Oncotarget*, **7**(29): 46545–46556.

Concordet JP, Haeussler M. 2018. CRISPOR: intuitive guide selection for CRISPR/Cas9 genome editing experiments and screens. *Nucleic Acids Research*, **46**(W1): W242–W245.

Cyphert HA, Walker EM, Hang Y, et al. 2019. Examining how the MAFB transcription factor affects islet β-cell function postnatally. *Diabetes*, **68**(2): 337–348.

Delano W. 2002. The PyMOL molecular graphics system.

de Mendoza A, Nguyen TV, Ford E, et al. 2022. Large-scale manipulation of promoter DNA methylation reveals context-specific transcriptional

responses and stability. *Genome Biology*, **23**(1): 163.
Dupree MA, Pollack SR, Levine EM, et al. 2006. Fibroblast growth factor 2 induced proliferation in osteoblasts and bone marrow stromal cells: a whole cell model. *Biophysical Journal*, **91**(8): 3097–3112.
Fukushima HS, Takeda H, Nakamura R. 2019. Targeted in vivo epigenome editing of H3K27me3. *Epigenetics & Chromatin*, **12**(1): 17.
Gao CX. 2021. Genome engineering for crop improvement and future agriculture. *Cell*, **184**(6): 1621–1635.
Gilbert LA, Larson MH, Morsut L, et al. 2013. CRISPR-mediated modular RNA-guided regulation of transcription in eukaryotes. *Cell*, **154**(2): 442–451.
Guo HY, Tang SB, Li LJ, et al. 2025. Gestational diabetes mellitus causes genome hyper-methylation of oocyte via increased EZH2. *Nature Communications*, **16**(1): 127.
Gupta D, Bhattacharjee O, Mandal D, et al. 2019. CRISPR-Cas9 system: a new-fangled dawn in gene editing. *Life Sciences*, **232**: 116636.
Haapaniemi E, Botla S, Persson J, et al. 2018. CRISPR-Cas9 genome editing induces a p53-mediated DNA damage response. *Nature Medicine*, **24**(7): 927–930.
Haleem-Smith H, Derfoul A, Okafor C, et al. 2005. Optimization of high-efficiency transfection of adult human mesenchymal stem cells in vitro. *Molecular Biotechnology*, **30**(1): 9–19.
Hall BG. 2013. Building phylogenetic trees from molecular data with MEGA. *Molecular Biology and Evolution*, **30**(5): 1229–1235.
Hu T M, Hsu S H, Tsai S M, et al. 2017. DNA methylation analysis of the EGR3 gene in patients of schizophrenia. *Psychiatry Research*, **251**: 115–117.
Huang YC, Chen WC, Yu CL, et al. 2023. FGF2 drives osteosarcoma metastasis through activating FGFR1-4 receptor pathway-mediated ICAM-1 expression. *Biochemical Pharmacology*, **218**: 115853.
Ito S, D'Alessio AC, Taranova OV, et al. 2010. Role of Tet proteins in 5mC to 5hmC conversion, ES-cell self-renewal and inner cell mass specification. *Nature*, **466**(7310): 1129–1133.
Iyer LM, Tahiliani M, Rao A, et al. 2009. Prediction of novel families of enzymes involved in oxidative and other complex modifications of bases in nucleic acids. *Cell Cycle*, **8**(11): 1698–1710.
Jin CF, Yan K, Wang MY, et al. 2023. Identification, characterization and functional analysis of fibroblast growth factors in black rockfish (*Sebastes schlegelii*). *International Journal of Molecular Sciences*, **24**(4): 3626.
Johnston RA, Aracena KA, Barreiro LB, et al. 2024. DNA methylation-environment interactions in the human genome. *eLife*, **12**: RP89371.
Kim BM, Kim J, Choi IY, et al. 2016. Omics of the marine medaka (*Oryzias melastigma*) and its relevance to marine environmental research. *Marine Environmental Research*, **113**: 141–152.
Koh KP, Yabuuchi A, Rao S, et al. 2011. Tet1 and Tet2 regulate 5-hydroxymethylcytosine production and cell lineage specification in mouse embryonic stem cells. *Cell Stem Cell*, **8**(2): 200–213.
Kohli RM, Zhang Y. 2013. TET enzymes, TDG and the dynamics of DNA demethylation. *Nature*, **502**(7472): 472–479.
Krejci P, Krakow D, Mekikian PB, et al. 2007. Fibroblast growth factors 1, 2, 17, and 19 are the predominant FGF ligands expressed in human fetal growth plate cartilage. *Pediatric Research*, **61**(3): 267–272.
Kuscu C, Arslan S, Singh R, et al. 2014. Genome-wide analysis reveals characteristics of off-target sites bound by the Cas9 endonuclease. *Nature Biotechnology*, **32**(7): 677–683.
Larson MH, Gilbert LA, Wang XW, et al. 2013. CRISPR interference (CRISPRi) for sequence-specific control of gene expression. *Nature Protocols*, **8**(11): 2180–2196.
Li JW, Shen ZK, Lin YS, et al. 2024a. DNA methylation of skeletal muscle function-related secretary factors identifies FGF2 as a potential biomarker for sarcopenia. *Journal of Cachexia, Sarcopenia and Muscle*, **15**(3): 1209–1217.
Li LC, Dahiya R. 2002. MethPrimer: designing primers for methylation PCRs. *Bioinformatics*, **18**(11): 1427–1431.
Li LK, Chen R, Zhang H, et al. 2024b. The epigenetic modification of DNA methylation in neurological diseases. *Frontiers in Immunology*, **15**: 1401962.
Liang F, Dong ZJ, Ye JM, et al. 2023. *In vivo* DNA methylation editing in zebrafish. *Epigenetics*, **18**(1): 2192326.
Liao HY, Wu JH, VanDusen NJ, et al. 2024. CRISPR-Cas9-mediated homology-directed repair for precise gene editing. *Molecular Therapy - Nucleic Acids*, **35**(4): 102344.
Lin SL, Ewen-Campen B, Ni XC, et al. 2015. *In vivo* transcriptional activation using CRISPR/Cas9 in *Drosophila*. *Genetics*, **201**(2): 433–442.
Liu XS, Wu H, Ji X, et al. 2016. Editing DNA methylation in the mammalian genome. *Cell*, **167**(1): 233–247. e17.
Liu XD, Ye CC, Wang Y, et al. 2025. DNA methylation confers a cerebellum-specific identity in non-human primates. *Zoological Research*, **46**(2): 414–428.
Livak KJ, Schmittgen TD. 2001. Analysis of relative gene expression data using real-time quantitative PCR and the 2^{-ddCT} method. *Methods*, **25**(4): 402–408.
Lotz S, Goderie S, Tokas N, et al. 2013. Sustained levels of FGF2 maintain undifferentiated stem cell cultures with biweekly feeding. *PLoS One*, **8**(2): e56289.
Lu SN, Wang JY, Chitsaz F, et al. 2020. CDD/SPARCLE: the conserved domain database in 2020. *Nucleic Acids Research*, **48**(D1): D265–D268.
Lu Y, Chen SR, Yang N. 2013. Expression and methylation of *FGF2, TGF-β* and their downstream mediators during different developmental stages of leg muscles in chicken. *PLoS One*, **8**(11): e79495.
Mani I. 2021. CRISPR-Cas9 for treating hereditary diseases. *Progress in Molecular Biology and Translational Science*, **181**: 165–183.
Mello B. 2018. Estimating TimeTrees with MEGA and the TimeTree resource. *Molecular Biology and Evolution*, **35**(9): 2334–2342.
Minh BQ, Schmidt HA, Chernomor O, et al. 2020. IQ-TREE 2: new models and efficient methods for phylogenetic inference in the genomic era. *Molecular Biology and Evolution*, **37**(5): 1530–1534.
Mojica EA, Kültz D. 2022. Physiological mechanisms of stress-induced evolution. *Journal of Experimental Biology*, **225**(S1): jeb243264.
Mossahebi-Mohammadi M, Quan MY, Zhang JS, et al. 2020. FGF signaling pathway: a key regulator of stem cell pluripotency. *Frontiers in Cell and Developmental Biology*, **8**: 79.
Nickle A, Ko S, Merrill AE. 2024. Fibroblast growth factor 2. *Differentiation*, **139**: 100733.
Nishida T, Kubota S, Aoyama E, et al. 2011. Effect of CCN2 on FGF2-induced proliferation and MMP9 and MMP13 productions by chondrocytes. *Endocrinology*, **152**(11): 4232–4241.
Nissen LJ, Cao RH, Hedlund EM, et al. 2007. Angiogenic factors FGF2 and PDGF-BB synergistically promote murine tumor neovascularization and metastasis. *The Journal of Clinical Investigation*, **117**(10): 2766–2777.
Nuñez JK, Chen J, Pommier GC, et al. 2021. Genome-wide programmable transcriptional memory by CRISPR-based epigenome editing. *Cell*, **184**(9): 2503–2519. e17.
Park H, Shin J, Kim Y, et al. 2022. CRISPR/dCas9-Dnmt3a-mediated targeted DNA methylation of *APP* rescues brain pathology in a mouse model of Alzheimer's disease. *Translational Neurodegeneration*, **11**(1): 41.
Qi LS, Larson MH, Gilbert LA, et al. 2013. Repurposing CRISPR as an RNA-guided platform for sequence-specific control of gene expression. *Cell*, **152**(5): 1173–1183.
Qian JM, Liu SX. 2024. CRISPR/dCas9-Tet1-mediated DNA methylation editing. *Bio-protocol*, **14**(8): e4976.
Qiu YR, Xu Q, Xie PC, et al. 2025. Epigenetic modifications and emerging therapeutic targets in cardiovascular aging and diseases. *Pharmacological Research*, **211**: 107546.
Rajalingam K, Schreck R, Rapp UR, et al. 2007. Ras oncogenes and their downstream targets. *Biochimica et Biophysica Acta (BBA) - Molecular Cell Research*, **1773**(8): 1177–1195.

Ramakrishnan S, Hu Q, Krishnan N, et al. 2017. Decitabine, a DNA-demethylating agent, promotes differentiation via NOTCH1 signaling and alters immune-related pathways in muscle-invasive bladder cancer. *Cell Death & Disease*, **8**(12): 3217.

Richter J, Stanley EG, Ng ES, et al. 2018. WNT9A is a conserved regulator of hematopoietic stem and progenitor cell development. *Genes*, **9**(2): 66.

Roddy KA, Prendergast PJ, Murphy P. 2011. Mechanical influences on morphogenesis of the knee joint revealed through morphological, molecular and computational analysis of immobilised embryos. *PLoS One*, **6**(2): e17526.

Roy Choudhury S, Heflin B, Taylor E, et al. 2023. CRISPR/dCas9-KRAB-mediated suppression of *S100b* restores p53-mediated apoptosis in melanoma cells. *Cells*, **12**(5): 730.

Sander JD, Joung JK. 2014. CRISPR-Cas systems for editing, regulating and targeting genomes. *Nature Biotechnology*, **32**(4): 347–355.

Shao CW, Li QY, Chen SL, et al. 2014. Epigenetic modification and inheritance in sexual reversal of fish. *Genome Research*, **24**(4): 604–615.

Shen B, Zhang WS, Zhang J, et al. 2014. Efficient genome modification by CRISPR-Cas9 nickase with minimal off-target effects. *Nature Methods*, **11**(4): 399–402.

Sinha S, Barbosa K, Cheng KY, et al. 2021. A systematic genome-wide mapping of oncogenic mutation selection during CRISPR-Cas9 genome editing. *Nature Communications*, **12**(1): 6512.

Song M, Gutzeit HO. 2003. Primary culture of medaka (*Oryzias latipes*) testis: a test system for the analysis of cell proliferation and differentiation. *Cell and Tissue Research*, **313**(1): 107–115.

Stemmer M, Thumberger T, del Sol Keyer M, et al. 2015. CCTop: an intuitive, flexible and reliable CRISPR/Cas9 target prediction tool. *PLoS One*, **10**(4): e0124633.

Sulzmaier FJ, Ramos JW. 2013. RSK isoforms in cancer cell invasion and metastasis. *Cancer Research*, **73**(20): 6099–6105.

Sun YX, Wang HY, Liu BH, et al. 2024. CRISPR/dCas9-mediated DNA methylation editing on *emx2* in Chinese Tongue Sole (*Cynoglossus semilaevis*) testis cells. *International Journal of Molecular Sciences*, **25**(14): 7637.

Szklarczyk D, Gable AL, Lyon D, et al. 2019. STRING v11: protein-protein association networks with increased coverage, supporting functional discovery in genome-wide experimental datasets. *Nucleic Acids Research*, **47**(D1): D607–D613.

Takahashi Y, Valencia MM, Yu Y, et al. 2023. Transgenerational inheritance of acquired epigenetic signatures at CpG islands in mice. *Cell*, **186**(4): 715–731. e19.

Tang YD, Guo JC, Wang TY, et al. 2018. CRISPR/Cas9-mediated 2-sgRNA cleavage facilitates pseudorabies virus editing. *The FASEB Journal*, **32**(8): 4293–4301.

Tsai SQ, Wyvekens N, Khayter C, et al. 2014. Dimeric CRISPR RNA-guided FokI nucleases for highly specific genome editing. *Nature Biotechnology*, **32**(6): 569–576.

Vojta A, Dobrinić P, Tadić V, et al. 2016. Repurposing the CRISPR-Cas9 system for targeted DNA methylation. *Nucleic Acids Research*, **44**(12): 5615–5628.

Vu TV, Doan DTH, Tran MT, et al. 2021. Improvement of the LbCas12a-crRNA system for efficient gene targeting in tomato. *Frontiers in Plant Science*, **12**: 722552.

Wang CK, Qu YH, Cheng JKW, et al. 2022a. dCas9-based gene editing for cleavage-free genomic knock-in of long sequences. *Nature Cell Biology*, **24**(2): 268–278.

Wang JY, Chitsaz F, Derbyshire MK, et al. 2023. The conserved domain database in 2023. *Nucleic Acids Research*, **51**(D1): D384–D388.

Wang SW, Gao C, Zheng YM, et al. 2022b. Current applications and future perspective of CRISPR/Cas9 gene editing in cancer. *Molecular Cancer*, **21**(1): 57.

Wang XG, Bhandari RK. 2020a. The dynamics of DNA methylation during epigenetic reprogramming of primordial germ cells in medaka (*Oryzias latipes*). *Epigenetics*, **15**(5): 483–498.

Wang XG, Bhandari RK. 2020b. DNA methylation reprogramming in medaka fish, a promising animal model for environmental epigenetics research. *Environmental Epigenetics*, **6**(1): dvaa008.

Waterhouse A, Bertoni M, Bienert S, et al. 2018. SWISS-MODEL: homology modelling of protein structures and complexes. *Nucleic Acids Research*, **46**(W1): W296–W303.

Wong TT, Collodi P. 2013. Effects of specific and prolonged expression of zebrafish growth factors, Fgf2 and Lif in primordial germ cells in vivo. *Biochemical and Biophysical Research Communications*, **430**(1): 347–351.

Wu HX, Chen YX, Wang ZX, et al. 2019. Alteration in TET1 as potential biomarker for immune checkpoint blockade in multiple cancers. *Journal for ImmunoTherapy of Cancer*, **7**(1): 264.

Wu TZ, Hu EQ, Xu SB, et al. 2021. clusterProfiler 4.0: a universal enrichment tool for interpreting omics data. *The Innovation*, **2**(3): 100141.

Xi YX, Li W. 2009. BSMAP: whole genome bisulfite sequence MAPping program. *BMC Bioinformatics*, **10**(1): 232.

Xu XB, Tan XY, Tampe B, et al. 2018. High-fidelity CRISPR/Cas9-based gene-specific hydroxymethylation rescues gene expression and attenuates renal fibrosis. *Nature Communications*, **9**(1): 3509.

Yasuda Y, Nishi N, Takahashi JA, et al. 1992. Induction of avascular yolk sac due to reduction of basic fibroblast growth factor by retinoic acid in mice. *Developmental Biology*, **150**(2): 397–413.

Yaylaoglu MB, Titmus A, Visel A, et al. 2005. Comprehensive expression atlas of fibroblast growth factors and their receptors generated by a novel robotic in situ hybridization platform. *Developmental Dynamics*, **234**(2): 371–386.

Yu GC, Wang LG, Han YY, et al. 2012. clusterProfiler: an R package for comparing biological themes among gene clusters. *OMICS: A Journal of Integrative Biology*, **16**(5): 284–287.

Yu HC, Huang FM, Lee SS, et al. 2016. Effects of fibroblast growth factor-2 on cell proliferation of cementoblasts. *Journal of Dental Sciences*, **11**(4): 463–467.

Zhang LY, Jia GX, Tao HP, et al. 2025. Maternal hypoxia exposure perturbs imprinted gene methylation in adult sperm and induces intergenerational placental impairments in male offspring. *Zoological Research*, **46**(6): 1273–1288.

Zhang WW, Chen HQ, Liu W, et al. 2024a. Characterizing marine medaka (*Oryzias melastigma*) haploid embryonic stem cells: a valuable tool for marine fish genetic research. *Animals*, **14**(18): 2739.

Zhang XY, Bhattacharya A, Pu CX, et al. 2024b. A programmable CRISPR/dCas9-based epigenetic editing system enabling loci-targeted histone citrullination and precise transcription regulation. *Journal of Genetics and Genomics*, **51**(12): 1485–1493.

Zhao BN, Yu XW, Shi JT, et al. 2024. A stepwise mode of TGFβ-SMAD signaling and DNA methylation regulates naïve-to-primed pluripotency and differentiation. *Nature Communications*, **15**(1): 10123.

Zhao FY, Xu SL, Zhang CF, et al. 2021. PDGF mediates pulmonary arterial smooth muscle cell proliferation and migration by regulating NFATc2. *Molecular Medicine Reports*, **23**(1): 39.

Zheng X, Huang CH, Yan S, et al. 2025. Advances and applications of genome-edited animal models for severe combined immunodeficiency. *Zoological Research*, **46**(1): 249–260.

Zhou YY, Zhou B, Pache L, et al. 2019. Metascape provides a biologist-oriented resource for the analysis of systems-level datasets. *Nature Communications*, **10**(1): 1523.